Traceability and uncertainty of defects automated measurements by CNN-powered Machine Vision Systems

CIRP Annals - Manufacturing Technology 74 (2025) 661–665

Contents lists available at ScienceDirect

CIRP Annals - Manufacturing Technology

journal homepage: https://www.editorialmanager.com/CIRP/default.aspx

Traceability and uncertainty of defects automated measurements by CNN-powered Machine Vision Systems

Giacomo Maculotti, Lorenzo Giorio, Gianfranco Genta, Maurizio Galetto (2)*

Department of Management and Production Engineering, Politecnico di Torino, Corso Duca degli Abruzzi 24, 10129 Turin, Italy

ARTICLE INFO

Article history:
Available online 19 April 2025

Keywords:
Visual inspection
Uncertainty
Convolutional neural network (CNN)

ABSTRACT

Surface geometric imperfections can be automatically inspected by machine vision systems. State-of-the-art applications prefer resorting to image analysis by Convolutional Neural Networks (CNNs), rather than traditional traceable inspection methods. CNNs have the advantage of greater speed, flexibility and automation but lack traceability, thus hindering quantitative quality controls and tolerances verification. This work proposes a methodology to estimate the uncertainty of automated measurements of surface geometrical imperfections based on CNNs while establishing traceability by leveraging on a photogrammetric system. The methodology is demonstrated on a gas metal arc welding of aluminium alloys for inspecting and measuring the quality of surface pores.

1. Introduction

On-machine measurements allow integrated metrology to identify defects and verify tolerances, enabling closed-loop feedback control of the manufacturing process by means of non-destructive quality controls [1], thus fostering sustainable manufacturing [2]. Tolerance verification within a metrological framework requires traceability and measurement uncertainty evaluation [3]. Integrated metrology often controls quality of part geometry and dimensions, leveraging optical inspection techniques, which grant suitable flexibility and speed to cope with stringent and increasing demand of high production efficiency.

Functionality of component is controlled by its surface layer properties [4], and the presence of geometrical imperfections can be detrimental for the application [5]. Thus, the inspection of surfaces' geometrical imperfections is of primary relevance and is typically carried out by visual inspection [6]. Automated visual inspection based on machine vision systems (MVSs) have been developed to overcome limits inherent in human visual inspection due to operators' poor reproducibility [6]. MVSs consists of hardware capable of producing images and of a software processing pipeline of such images. MVSs find widespread application in assembly, e.g. for part presence and orientation recognition [7], and manufacturing processes for in-line quality controls, e.g. in electronics for geometry and surface geometrical imperfections of printed circuit board and MEMS, e.g. delamination, pores, scratches [8], and in welding processes, for monitoring the geometry of the weld seam [9], molten pool and keyhole, and to detect the presence of spatter and droplets [10].

Most conventional analysis of images collected by MVSs relies on the application of a set of preprocessing, enhancement, and filtering steps [11] possibly aided by various measurement conditions, e.g., bright and dark field, structured illumination [12]. Such set of very complex operations can isolate specific features of the image, ultimately detecting and classifying imperfections [6]. More recently, thanks to Machine Learning and enabling technology as high-performance and edge computing, learning approaches have been introduced to identify and classify defects [13]. Learning approaches mostly leverage Convolutional Neural Networks (CNNs) and provide greater flexibility in handling complex detection problem by dispensing the end user with the complex tasks of a priori designing the most apt set of preprocessing and filtering pipelines [13,14].

Visual inspections should be distinguished in those aimed at the detection and those at the measurement. In fact, despite surface geometric imperfection detection is essential, the measurement step is critical because in several applications, e.g. arc and laser welding [15], an imperfection is considered a defect only if it exceeds specific sizes [6]. Consequently, measuring the detected imperfections and evaluating the measurement uncertainty [16], by propagating relevant contributions, are mandatory to perform quantitative quality control and tolerance verification [17], to reduce waste, unnecessary quality costs related to I type errors, i.e., false positives, and image loss costs due to poor quality related to II type errors, i.e., false negatives. Accordingly, metrological measurement systems more advanced than 2D-cameras and capable of measuring topographical maps or point clouds are needed to achieve actual measurements suitable for tolerance verification. Such approaches might require extremely complex processing pipeline basing on curvature [18] and topography segmentation [19], and are typically more expensive and time consuming than CNN applied to 2D images. Furthermore, CNNs were originally conceived for object detection, which does not allow object dimensions measurement. Despite alternative routes for quality controls based on CNN features have been proposed [20], they do

* Corresponding author.
E-mail address: maurizio.galetto@polito.it (M. Galetto).

https://doi.org/10.1016/j.cirp.2025.03.023

not target the measurand and hence do not allow for tolerance verification. Conversely, the recent development of semantic segmentation, i.e. the extraction of edges of the detected object [13], enabled the application of CNNs for surface geometric imperfection characterisation towards quality control and tolerance verification. The seminal paper of Wolfschläger et al. [14] provided a first attempt of imperfection measurement on blanked components by semantic segmentation. The possibility of implementing CNNs also for measuring identified imperfections would allow a simpler alternative to other measurement systems, e.g. for point cloud acquisition.

However, machine vision cameras typically adopted for imperfection segmentation are not actual measuring instruments [21]. Furthermore, the literature tends to calibrate camera pixel size with calibrated object micrometers [14,22] to obtain the scale conversion factor to allow metric measurements. Such simplistic approach neglects correcting optical aberrations, e.g. barrelling and pin-cushion distortion typical of cameras, and sine errors, which are due to the working distance of the objective lens from the measurand and are critical and liable of severely amplifying the bias due to distortions, if the relative position of measurand and the camera is not highly precise and repeatable, condition hardly achievable for in-line process control. Last, typical metrics of CNN performances [13], e.g. Recall and Intersection-over-Union (IoU), are not useful to describe metrological characteristics, e.g. accuracy and precision [21], of the overall MVS for the measurement task. Mizutani et al. [23] first attempted to estimate prediction uncertainty of NN, overcoming limits of conventional metrics, and to optimize the NN structure.

This work, in Section 2, proposes a methodology to establish traceability of MVS with a 2D-camera and CNN for segmentation and automated measurements of surface geometrical imperfections. Innovatively, this work introduces a method to estimate the measurement uncertainty of MVS segmentation and measurement task. Section 3 demonstrates the methodology on gas metal arc welding case study for surface pores measurement on hybrid aluminium joints. Section 4 draws conclusions.

2. Methodology

Fig. 1 outlines the proposed data workflow in the designed MVS. Differently from related literature [6,14], multiple images of the component are collected by the MVS camera and are processed in parallel by photogrammetry and by an ad-hoc trained CNN.

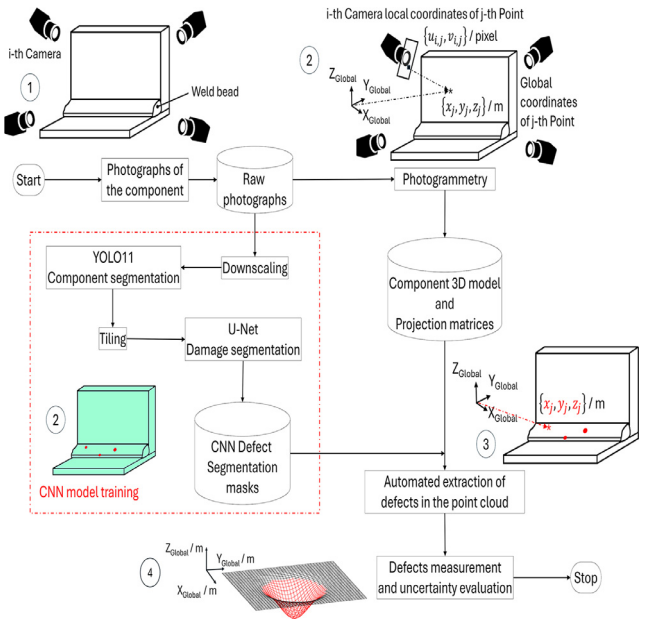

Fig. 1. Flowchart of the proposed approach for automated segmentation and measurement of surface geometrical imperfections on a weld bead. Most relevant steps are highlighted: photographing the component (1), photogrammetric construction of the metric point cloud and defect segmentation by CNN, performed contemporarily (2), the automated extraction of the defects in the point cloud (3) and the measurement (4).

Multiple images can be obtained by relative repositioning of the camera and the component limiting the application to in-line post-process integrated metrology [3].

The most severe limitation of state-of-the-art solution, hindering measurements of segmented surface geometrical imperfections, lies in the calibration of camera of the MVS, as discussed in Section 1. This work proposes to leverage photogrammetry to calibrate scale and distortion parameters of the MVS camera to correct systematic errors. The collected multiple images are exploited to solve collinearity equations and self-calibrate [24] camera distortion parameters, accounting for radial, tangential, and skewness distortions [25]. Photogrammetry allows to obtain metric dimensions while correcting for systematic optical errors. The photogrammetric system allows metrological characterisation of the segmented imperfections. Furthermore, the photogrammetric system calibration allows establishing traceability for the MVS. This can be obtained by measuring with the photogrammetric system an artefact calibrated with a Coordinate Measuring Machine (CMM) [26]. Accordingly, the surface imperfection standard uncertainty contribution of the photogrammetric system,u_{Photo}, includes several contributions combined as per the Law of Propagation of Uncertainty (LPU) [16]:

$$u^2_{Photo} = u^2_{Trac} + \frac{\bar{e}^2_{Photo}}{3} + s^2(e_{Photo}) + u^2_{fit,\ Photo} \tag{1.1}$$

$$u^2_{Trac} = \frac{MPE^2_{CMM}}{3} + s^2_{calib} + u^2_{Measurand} \tag{1.2}$$

Firstly, the traceability u_{Trac}, catering for the uncertainty of the CMM calibration of the artefact. This includes: the CMM accuracy, estimated from the Maximum Permissible Error (MPE) and propagated as a Type B contribution with a uniform distribution; the reproducibility of the calibration s_{calib}, i.e. the standard deviation of replicated measurements of the reference measurand with the CMM; and contributions due to the variation of the measured workpiece $u_{Measurand}$, e.g. form deviation [26,27]. Secondly, the metrological characteristics of the photogrammetric system, estimated from replicated measurements in reproducibility conditions, e.g. changing the illumination, the number of images and the relative position of the reference artefact with respect to the camera [26]. In particular, the accuracy can be propagated from the average measurement error $\bar{e}_{Photo}$, with respect to the CMM calibration, with a uniform distribution; the reproducibility as the standard deviation of such error $s(e_{Photo})$; also, the random error of any fitting needed for the feature measurement shall be included $u_{fit,Photo}$, e.g. as the residuals standard deviation.

Conversely, the CNN allows segmenting imperfections, i.e. isolating in each image the pixels relevant to the surface imperfection. In the next processing step, as depicted in Fig. 1, segmented pixels are input in the calibrated collinearity equations to obtain metric point clouds of the surface geometric imperfection, i.e. set $\boldsymbol{P}$ of cartesian triples $p_i = \{x_i, y_i, z_i\}$. Such point clouds can be exploited to measure relevant dimensions.

The imperfection segmentation can be trained, following most common state-of-the-art best practices, by transfer learning of pre-existing CNN, e.g. U-Net [13,14]. This is performed by feeding to the CNN a set of marked images highlighting the position of the imperfections by expert operators, i.e. *ground truth* (GT) masks. Transfer learning modifies the weights of the network to minimize a loss function. Typical performance indicators are the number of the true positive (TP), true negative (TN), false positive (FP), and false negative (FN) recognitions. It is worth noticing that FP are I type errors, and FN are II type errors. Such metrics, computed pixel-wise, are customarily aggregated in indexes typical in Machine Learning, e.g. the segmentation precision $Prec_{seg} = TP/(TP + FP)$, the recall or true positive rate $TPR = TP/(TP + FN)$, the $IoU = TP/(TP + FN + FP)$, and the *Dice loss* $= 1 - (2 \cdot IoU)/(1 + IoU)$ [13]. Although such metrics are useful to summarize aggregated performances, they are not readily exploitable for metrological applications. Conversely, leveraging the proposed workflow, described in Fig. 1, it is possible to compare the point clouds of the imperfections segmented based on the GT mask, $\boldsymbol{P}_{GT}$, and the predicted mask, $\boldsymbol{P}_{CNN}$, which are sets with cardinality $\#(\boldsymbol{P}_{GT}) = m$ and $\#(\boldsymbol{P}_{CNN}) = n$. Let the point-to-point cloud distances be

$d_{i,CNN} = \min_{j=1,\dots,m} (||p_{i,CNN} - p_{j,GT}||_2)$ and $d_{j,GT} = \min_{i=1,\dots,n} (||p_{j,GT} - p_{i,CNN}||_2)$, where the $\|\blacksquare\|_2$ operator indicates the L-2 norm, i.e. the Euclidean distance. For how the distances have been built, d_{CNN} includes errors due to FP and d_{GT} due to FN. The mixture d of d_{CNN} and d_{GT} caters for both systematic errors and random errors of the model. Thus, it allows estimating the metrological accuracy and precision due to the CNN segmentation, respectively, as the average $\overline{d}$ and standard deviation $s(d)$ of the distances. The standard uncertainty due to the segmentation, i.e. the CNN, u_{CNN} can be written as:

$$u_{CNN}^2 = \frac{\overline{d}^2}{3} + s^2(d) \tag{2.1}$$

$$\overline{d} = \frac{\#(\boldsymbol{d}_{CNN})}{\#(\boldsymbol{d}_{CNN}) + \#(\boldsymbol{d}_{GT})}\overline{d_{CNN}} + \frac{\#(\boldsymbol{d}_{GT})}{\#(\boldsymbol{d}_{CNN}) + \#(\boldsymbol{d}_{GT})}\overline{d_{GT}} \tag{2.2}$$

$$s^2(d) = \left(\frac{(\boldsymbol{d}_{CNN})}{(\boldsymbol{d}_{CNN}) + (\boldsymbol{d}_{GT})}\right)^2 s^2(d_{CNN}) + \left(\frac{(\boldsymbol{d}_{GT})}{(\boldsymbol{d}_{CNN}) + (\boldsymbol{d}_{GT})}\right)^2 s^2(d_{GT}) \tag{2.3}$$

The combined standard uncertainty of the MVS $u_{c,MVS}$ can be computed compounding contributions from both the measurement, i.e. the photogrammetric camera system, and the segmentation part:

$$u_{c,MVS} = \sqrt{u_{Photo}^2 + u_{CNN}^2} \tag{3}$$

3. Case study

The methodology proposed in Section 2 is applied to a case study for the quality control of a specific type of surface geometric imperfections in gas metal arc welding (GMAW) [28]. GMAW is largely the object of the application of MV inspection [10] and of in-line integrated metrology to achieve real-time control of the process [9]. Current challenges include welding of different materials or materials coming from different manufacturing processes [29]. Surface pores, i.e. *gas pores that break the surface of the weld* [30], are particularly critical for they can act as seeding points for cracks propagation. Not all pores present on the surface, i.e. geometric imperfections, have to be considered defects. The maximum tolerable size of surface pores depends on the required weld bead quality. Thus, they represent a suitable example of imperfection whose identification is not sufficient to determine the presence of a defect, but they require a measurement.

3.1. Materials and experimental setup

In this work, the proposed methodology is applied to inspect the quality of surface pores on a cast aluminium on rolled aluminium corner joint for automotive applications. The most significant challenge lies in the risk of generating large surface pores when the welding interacts with inherent internal porosities of the cast component. Six parts, shown in Fig. 2(a), with different length parallel to the weld bead were manufactured at the J-Tech laboratory of Politecnico di Torino. The rolled aluminium sheet has the smallest thickness, i.e. 3 mm. The joint features a corner joint geometry with a nominal weld bead throat thickness of the fillet weld of 4 mm. In such a condition, to ensure the maximum weld quality, i.e. quality level *B*, the maximum tolerable surface pore shall not exceed 0.4 mm [15]. Thus, the expanded uncertainty shall not exceed 33% of the maximum tolerable dimension, i.e. 0.133 mm, to ensure adequate tolerance verification [17].

The photogrammetric setup, see Fig. 2(c), includes a rotary table, and one camera Olympus OM-D E-M5 II equipped with an Olympus 14–150 mm f4–5.6 M.ZUIKO lens. Images were taken at a distance of about 50 cm from the component, with a resolution of (4608×3456) pixel. The rotary table features markers whose positions were calibrated, to allow collinearity equation scale parameters calibration [25], by a Hexagon Global Image 070707 CMM (MPE of 1 µm) with 5 replications by 2 operators showing a standard deviation of 1 µm. Photogrammetric reconstruction was performed relying on the Python library of Agisoft© Metashape. The calibration artefact was a turned aluminium step (diameter of 50 mm), see Fig. 2(b), with the smallest step of 1.447 mm, calibrated with the CMM.

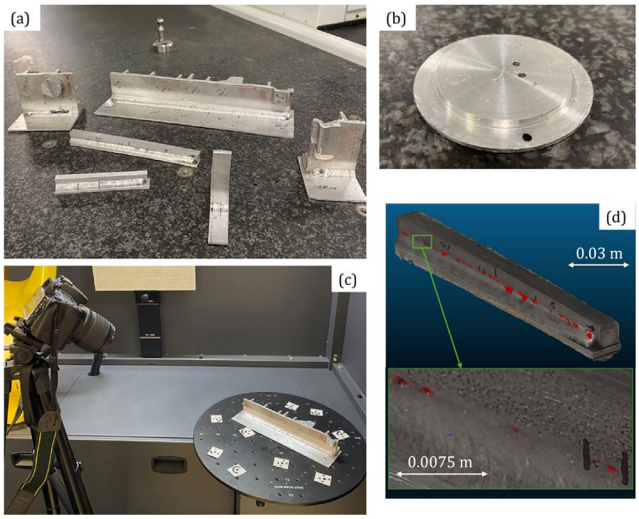

Fig. 2. (a) Arc welded parts. (b) Calibration artefact. (c) Experimental setup: camera and rotary table. (d) Reconstructed mesh of the point cloud by photogrammetry, with CNN-segmented surface pores shown in red and green inset at higher magnification.

3.2. Photogrammetric system calibration

The photogrammetric system setup, hosted in the metrological room of Mind4Lab at DIGEP – Politecnico di Torino, was calibrated to evaluate uncertainty contribution reported in Eq. (1). The reference artefact thickness was calibrated by randomly measuring 16 points on each opposing plane six times. The contributions due to the traceability, evaluated according to the methodology outlined in Section 2, are reported in Table 1. The variability due to the measurand was estimated as a type B contribution from the range of the residuals of the fitting for the planarity. Then, the photogrammetric system metrological performance was evaluated. Specifically, two camera poses, with and without artificial illumination, were used to take 68 pictures of the calibration artefact. The average error $\overline{e}_{Photo}$ resulted of 82.7 µm, making the accuracy the most relevant contribution, while other contributions are shown in Table 1.

Table 1
Uncertainty contribution of the MV photogrammetric system.

	$MPE_{CMM}/\sqrt{3}$	s_{calib}	$u_{Measurand}$
	0.6 µm	1.6 µm	4.5 µm
u_{Trac}		4.8 µm	
	$\overline{e}_{Photo}/\sqrt{3}$	$s(e_{Photo})$	$u_{fit,Photo}$
	48.0 µm	15.0 µm	8.3 µm
u_{Photo}		50.9 µm	

3.3. CNN training

A dataset of 451 images was collected and manually annotated to generate GT segmentation masks for each image, indicating the component and the surface pores. The dataset was split with a 80%–10%–10% ratio for training, validation and testing. The surface pore identification was implemented as a series of two segmentation CNN models (see Fig. 3). Firstly, a YOLO11 [31] for instance segmentation was trained to segment the component. Training aimed to minimize a composed loss function (box, segmentation, classification, and distribution focal losses), resulting in an IoU on the test set of 0.9. The segmentation masks thus created were used to reduce the image size to the second CNN requirement size without sacrificing the resolution by isolating the component and then creating a tiled layout of (1024×1024) pixel tiles, resulting in a final dataset consisting of 1345 tiles. On such dataset, the surface pore segmentation was performed using a U-Net network with ResNet-18 encoder [13]. The U-Net was trained to minimize the Dice loss. Table 2 reports the training hyperparameters for both models. Data augmentation of the training dataset was performed using the Albumentations Python library. Images were randomly flipped horizontally, vertically or

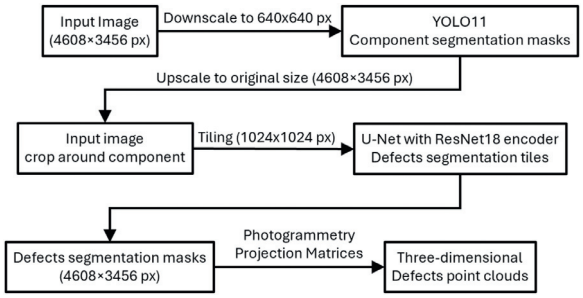

Fig. 3. Architecture of the CNN surface pore identification workflow used, based on two CNN segmentation models running in series.

Table 2
Hyperparameters for the YOLO11 and U-Net networks.

Hyperparameters	YOLO11m-seg [31]	U-Net [13]
Image size	(640×640) px	(1024×1024) px
Pre-training dataset	COCO-Seg	ImageNet
Epochs	250	150
Batch size	10	8
Optimizer	AdamW (learning rate=2e-3, momentum=0.9)	Adam (learning rate=5e-4)
Learning rate	0.01	5e-4
Validation metric	Precision, Recall, mean Average Precision	IoU, Precision, Recall

rotated, to remove possible bias of the segmentation network to learn pattern based on the component orientation which should not influence the segmentation; similarly, random modifications to brightness, hue and saturation were applied to simulate different lighting configurations during images acquisition.

The implementation, training and evaluation of the whole CNN framework was performed using PyTorch 2.1.1+cu121 and Python 3.11, on a Linux machine with one NVIDIA Quadro P5000 and 16 GB of VRAM. Training for the YOLO11 network took around 33 s/epoch, and 125 s/epoch for the U-Net. Fig. 4 shows the evolution reaching stabilization of the training loss and validation metrics during training for the U-Net. Using the trained models, the surface pores segmentation for each image can be performed. The binary masks thus created can be transformed into three-dimensional point clouds through the photogrammetry projection matrices per each image. Point-to-point cloud distances are evaluated to estimate metrological performances of the trained CNN. According to Section 2, the distance error resulted with average $\bar{d} = 8.1$ µm and standard deviation $s(d) = 41.8$ µm. This yielded an overall standard uncertainty contribution of the pore dimension measurement due to the segmentation of u_{CNN} of 42.1 µm.

3.4. Results discussion

Fig. 2(d) shows the point cloud of a component with the highlighted automatically segmented surface pores thanks to the CNN. Combining the photogrammetric system and the segmentation uncertainty contribution, a combined standard uncertainty of the

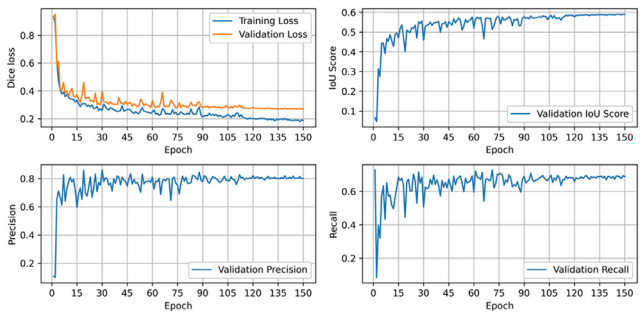

Fig. 4. Loss function and metrics during training of the U-Net network.

Table 3
MVS metrological performance comparison for GMAW surface pore automated measurement. Quality level as per ISO 10042:2018 [15].

Camera	Basler		Olympus	
u_{Photo} / µm	50.8		50.9	
CNN	LinkNet	U-Net	LinkNet	U-Net
IoU	0.704	0.694	0.658	0.665
u_{CNN} / µm	129.9	80.5	54.4	42.1
U_{MVS} / µm	279.0	190.4	149.0	132.2
Quality Level	D	C	C	B

MVS $u_{c,MVS}$ resulted of 66.1 µm. Thus, a measurement uncertainty with a coverage factor $k = 2$, results of $U_{MVS} = 132.2$ µm, suitable for tolerance verification of the considered measured task. Furthermore, the proposed methodology allows comparing performances of different MVSs within a metrological framework. In particular, the presented methodology was applied to the same case study, considering a combination of two alternative cameras, i.e. the already mentioned Olympus and a machine vision camera Basler acA2500−14uc with lower resolution [26] for the photogrammetric system, with two alternative CNNs for the pore segmentation, i.e. the U-Net and the LinkNet (with Resnet18 encoder) [13,14]. Results are summarised in Table 3, showing that both contribution of the photogrammetric system, i.e. the metrological measuring instrument, and the CNN impact on the overall uncertainty. Also, results highlight that, with similar metrological performance of the photogrammetric system, despite the comparable IoU, the significantly different pixel resolution greatly affects overall performances.

4. Conclusions

This work proposed a methodology to establish traceability of automated defects identification in MVS by coupling photogrammetry and CNN. Innovatively, thanks to the use of photogrammetry, traceable measurements of segmented defects by CNN were achieved. Thanks to the introduced methodology, uncertainty evaluation combining contribution from both the measurement and the segmentation was performed. The proposed methodology was applied to a case study to verify the quality of arc welding of aluminium joints, while proving capable of comparing metrological performances of different MVS solutions. Future works will focus on improving measurement uncertainty of the MVS, on testing the methodology on components with known and calibrated defects and on applying the methodology to multiple imperfections including a classification task.

Declaration of interests

The authors declare that they have no known competing financial interests or personal relationships that could have appeared to influence the work reported in this paper.

CRediT authorship contribution statement

Giacomo Maculotti: Writing – original draft, Visualization, Validation, Methodology, Investigation, Formal analysis, Conceptualization. **Lorenzo Giorio:** Writing – original draft, Visualization, Software, Methodology, Data curation. **Gianfranco Genta:** Writing – review & editing, Validation, Methodology, Formal analysis. **Maurizio Galetto:** Writing – review & editing, Validation, Supervision, Resources, Project administration, Funding acquisition, Conceptualization.

Acknowledgments

This work was funded by 23IND08 DI-Vision grant by European Partnership on Metrology and EU Horizon Europe Research and Innovation Programme.

References

[1] Gao W, Haitjema H, Fang FZ, Leach RK, Cheung CF, Savio E, Linares JM (2019) *On-machine and in-process surface metrology for precision manufacturing*, CIRP Annals – Manufacturing Technology. 843–866.
[2] Duflou JR, Sutherland JW, Dornfeld D, Herrmann C, Jeswiet J, Kara S, Hauschild M, Kellens K (2012) *Towards energy and resource efficient manufacturing: A processes and systems approach*, CIRP Annals – Manufacturing Technology. 587–609.
[3] Archenti A, Gao W, Donmez A, Savio E, Irino N (2024) *Integrated metrology for advanced manufacturing*, CIRP Annals – Manufacturing Technology. 639–665.
[4] Schulze V, Aurich J, Jawahir IS, Karpuschewski B, Yan J (2024) *Surface conditioning in cutting and abrasive processes*, CIRP Annals – Manufacturing Technology. 667–693.
[5] Bruzzone AAG, Costa HL, Lonardo PM, Lucca DA (2008) *Advances in engineered surfaces for functional performance*, CIRP Annals – Manufacturing Technology. 750–769.
[6] Mullany B, Savio E, Haitjema H, Leach R (2022) *The implication and evaluation of geometrical imperfections on manufactured surfaces*, CIRP Annals – Manufacturing Technology. 717–739.
[7] Puttero S, Verna E, Genta G, Galetto M (2024) Impact of product family complexity on process performance in electronic component assembly. *International Journal of Advanced Manufacturing Technology* 132:2907–2922.
[8] Huang SH, Pan YC (2015) Automated visual inspection in the semiconductor industry: a survey. *Computers in Industry* 66:1–10.
[9] Wang P, Kershaw J, Russell M, Zhang J, Zhang Y, Gao RX (2022) *Data-driven process characterization and adaptive control in robotic arc welding*, CIRP Annals – Manufacturing Technology. 45–48.
[10] Fan X, Gao X, Liu G, Ma N, Zhang Y (2021) Research and prospect of welding monitoring technology based on machine vision. *International Journal of Advanced Manufacturing Technology* 115:3365–3391.
[11] Hassanin AAIM, Abd El-Samie FE, El Banby GM (2019) A real-time approach for automatic defect detection from PCBs based on SURF features and morphological operations. *Multimed Tools Appl* 78:34437–53447.
[12] Pfeifer T, Wiegers L (1998) Adaptive control for the optimized adjustment of imaging parameters for surface inspection using machine vision. *CIRP Annals* : 487–490. 47/1.
[13] Zaidi SSA, Ansari MS, Aslam A, Kanwal N, Asghar M, Lee B (2022) A survey of modern deep learning based object detection models. *Digital Signal Processing: A Review Journal* 126:103514.
[14] Wolfschläger D, Woltersmann JH, Montavon B, Schmitt RH (2022) Sheared edge defect segmentation using a convolutional U-net for quantified quality assessment of fine blanked workpieces. *Precision Engineering* 75:129–141.
[15] ISO 10042 (2018) *Welding - Arc-welded joints in aluminium and its alloys-Quality levels for imperfections*, ISO, Genève (CH).
[16] JCGM100 (2008) *Evaluation of measurement data — Guide to the expression of uncertainty in measurement (GUM)*, JCGM, Sèvres (FR).
[17] ISO 14253-1 (2017) *Geometrical product specifications (GPS) — Inspection by measurement of workpieces and measuring equipment*, ISO, Genève (CH).
[18] Jiang X, Senin N, Scott PJ, Blateyron F (2021) *Feature-based characterisation of surface topography and its application*, CIRP Annals – Manufacturing Technology. 681–702.
[19] Genta G, Maculotti G (2021) *Uncertainty evaluation of small wear measurements on complex technological surfaces by machine vision-aided topographical methods*, CIRP Annals – Manufacturing Technology. 451–454.
[20] Schmitt RH, Wolfschläger D, Masliankova E, Montavon B (2022) *Metrologically interpretable feature extraction for industrial machine vision using generative deep learning*, CIRP Annals – Manufacturing Technology. 433–436.
[21] JCGM 200 (2012) *International vocabulary of metrology (VIM)*, JCGM, Sèvres (FR).
[22] Dai Y, Zhu K (2018) A machine vision system for micro-milling tool condition monitoring. *Precision Engineering* 52:183–191.
[23] Mizutani Y, Kataoka S, Nagai Y, Uenohara T, Takaya Y (2022) *Structure estimation of deep neural network for triangulation displacement sensors*, CIRP Annals – Manufacturing Technology. 425–428.
[24] Fraser CS (1997) Digital camera self-calibration. *ISPRS Journal of Photogrammetry and Remote Sensing* : 149–159. 52/4.
[25] Schmitt RH, Peterek M, Morse E, Knapp W, Galetto M, Härtig F, Goch G, Hughes B, Forbes A, Estler WT (2016) *Advances in Large-Scale Metrology – Review and future trends*, CIRP Annals – Manufacturing Technology. 643-265. 65/2.
[26] Trombini M, Maculotti G, Maisano DA, Pagani A, Franceschini F (2025) Scaling photogrammetry: a comparative evaluation and metrological assessment across small- and meso-scale domains. *Precision Engineering* 92:124–140.
[27] ISO 15530-3 (2011) *Geometrical product specifications (GPS) - Coordinate measuring machines (CMM): Technique for determining the uncertainty of measurement. Part 3: Use of calibrated workpieces or measurement standards*, ISO, Genève (CH).
[28] Lanzetta M, Santochi M, Tantussi G (2001) *On-line control of robotized Gas Metal Arc Welding*, CIRP Annals. 13–16.
[29] Yang J, Oliveira JP, Li Y, Tan C, Gao C, Zhao Y, Yu Z (2022) Laser techniques for dissimilar joining of aluminum alloys to steels: a critical review. *Journal of Material Processing Technology* 301:117443.
[30] ISO 6520-1 (2007) *Welding and allied processes - Classification of geometric imperfections in metallic materials. Part 1: Fusion welding*, ISO, Genève (CH).
[31] Khanam, R., Hussain, M., 2024, YOLOv11: an overview of the key architectural enhancements, arXiv. doi: 10.48550/arXiv.2410.17725.